Global Fluid Power Society PhD Symposium 2022| Naples, Italy - 2022

Cartesian Damping Controller with Nonlinear Control for a Floating-Base Hydraulic Manipulator

Pauli Mustalahti and Jouni Mattila

Faculty of Engineering and Natural Sciences, Tampere University, Finland,
pauli.mustalahti@tuni.fi
Faculty of Engineering and Natural Sciences, Tampere University, Finland,
jouni.mattila@tuni.fi

Abstract

Hydraulic manipulators are widely used to move loads to the desired position in many industrial sectors. Specifically, in the forestry, mining, and construction industries, a rigid hydraulic manipulator is mounted on a moving wheeled or tracked platform. These mobile manipulators extend the working envelope of the manipulator due to the mobility of the platform. Common to these industrial applications is that the uneven terrain conditions of the environment cause the manipulator to float. Considering the coupled and nonlinear dynamics behavior of the mobile platform and the rigid manipulator, designing a high-performance closed-loop controller is challenging. In this paper, our main focus is to define the control equations of the model-based Virtual Decomposition Control (VDC) approach to handle mobile manipulator platform movements during the manipulator end-effector motions. As a novel feature, VDC allows control design locally at the subsystem level without imposing additional approximations. The simulation results with a 3-Degrees-of-freedom (DOF) hydraulic manipulator mounted on a floating base are used to demonstrate the effectiveness of the proposed controller.

1 Introduction

Heavy-duty articulated hydraulic manipulators are widely used in industrial applications to transfer heavy loads to desired locations. For industrial applications, it is typical that a rigid hydraulic manipulator is mounted on a moving platform. A non-fixed manipulator base enables extension of the work envelope and the functionality of the manipulator compared to the fixed-base system. Therefore, the combined manipulator and the moving platform are operated as a mobile manipulator. Considering mobile manipulator operations, the working envelope typically consists of uneven terrain conditions (e.g., in the forest, mining and ship industries). Due to the mobile manipulator's complex dynamics and the strong coupling between the mobile platform and the manipulator, designing a closed-loop control and operating these systems are difficult tasks [2, 4].

Decreased human operator workload, energy efficiency, and manipulator safety can be improved by using semi-automated operations. For these reasons, hydraulic manipulator robotic closed-loop control and more automatic operations are currently an important research topic [1, 13]. The first commercial resolved-rated controlled hydraulic manipulators are already available [3, 18] for forest log loading and harvesting applications. However, these commercial solutions typically do not consider the manipulator floating-base movements during the operations. For this reason, manipulator end-effector control is sensitive to platform movements. The majority of the proposed anti-sway control methods for hydraulic heavy-duty manipulators in the literature [5, 14, 17, 19] demonstrates control methods for handling oscillation of the passive unactuated joints. However, in these methods the manipulator is assumed to be in a fixed position. This paper assumes that the motion of the floating base is known, and the uncertainty of the motion of the base can be further considered.

As reported in [13], nonlinear model-based (NMB) control designs have been shown to provide superior control performance for hydraulic manipulators versus the state-of-the-art methods presented. Due to the highly nonlinear dynamics behavior [20] of hydraulic systems, NMB control methods are needed. The Virtual Decomposition Control (VDC) approach, introduced in [21, 22], was reported to provide state-of-the-art control performance with hydraulically driven manipulators in [8, 10, 12]. The VDC controller for the 3-degrees-of-freedom (DOF) manipulator arm was presented in [15], and the VDC controller for the 6-DOF hydraulic manipulator was given in [16].

The main focus of this study is to extend the VDC approach to handle a control design for a floating-base hydraulic manipulator. In this study, it is assumed that the manipulator is placed on the floating-base. Considering the uneven terrain conditions for the mobile manipulator, the floating-base movements follow from the mobile manipulator platform movements. Therefore, it is also assumed that there are no actuators to compensate for the effects of the platform movements on the to manipulator base. The proposed control method effectiveness is verified by using simulation results with a 3-DOF hydraulic manipulator with a 6-DOF floating-base platform.

This paper is organized as follows. Section 2 briefly introduces the mathematical notations of the VDC approach. In Section 3, the virtual decomposition for the entire system is expressed. In addition, the kinematics modeling for the examined entire system is presented in Section 3. The control equations for the examined system are presented in Section 4. Finally, the experimental results are presented in Section 5, and conclusions are drawn in Section 6.

2 Mathematical Foundation

The mathematical notations of the VDC approach are defined as follows. Let us assume that successive orthogonal three-dimensional coordinate frames $\{\mathbf{A}\}$ and $\{\mathbf{B}\}$ are fixed to a rigid body. Then, restrictions [22] for these coordinate frames can be defined as

$$^{\mathbf{B}}V = {}^{\mathbf{A}}\mathbf{U}_{\mathbf{B}}^{T}\,{}^{\mathbf{A}}V \tag{1}$$

$$^{\mathbf{A}}F = {}^{\mathbf{A}}\mathbf{U}_{\mathbf{B}}\,{}^{\mathbf{B}}F, \tag{2}$$

where ${}^{\mathbf{A}}\mathbf{U}_{\mathbf{B}} \in \mathbb{R}^{6\times 6}$ is the force/moment transformation between two fixed coordinate frames. In Eq. (1), the linear/angular velocity vector ${}^{\mathbf{A}}V = [{}^{\mathbf{A}}\mathbf{v} \;\; {}^{\mathbf{A}}\omega]^T$ in coordinate frame $\{\mathbf{A}\}$ can be defined as a combination of the linear velocity vector and $\mathbf{v} \in \mathbb{R}^3$ and the angular velocity vector ${}^{\mathbf{A}}\omega \in \mathbb{R}^3$. Furthermore, the force/moment vector ${}^{\mathbf{A}}F = [{}^{\mathbf{A}}\mathbf{f} \;\; {}^{\mathbf{A}}\mathbf{m}]^T$ can be defined as a combination of the force vector ${}^{\mathbf{A}}\mathbf{f} \in \mathbb{R}^3$ and the moment vector ${}^{\mathbf{A}}\mathbf{m} \in \mathbb{R}^3$.

Furthermore, the dynamics of the rigid links described in coordinate frame $\{\mathbf{A}\}$ can be defined [22] as

$$^{\mathbf{A}}F^{*} = \mathbf{M}_{\mathbf{A}}\frac{d}{dt}({}^{\mathbf{A}}V) + \mathbf{C}_{\mathbf{A}}({}^{\mathbf{A}}\omega)\,{}^{\mathbf{A}}V + \mathbf{G}_{\mathbf{A}}, \tag{3}$$

where $\mathbf{M_A} \in \mathbb{R}^{6\times 6}$ denotes the mass matrix, $\mathbf{C_A}({}^{\mathbf{A}}\boldsymbol{\omega}) \in \mathbb{R}^{6\times 6}$ denotes the Coriolis and centrifugal terms, ${}^{\mathbf{A}}F^* \in \mathbb{R}^6$ denotes the net force/moment vector, and $\mathbf{G_A} \in \mathbb{R}^6$ denotes the gravity vector.

In a control design, the required rigid body dynamics can be defined with the linear parameterization expression as

$$\mathbf{Y_A}\theta_{\mathbf{A}} \overset{\text{def}}{=} \mathbf{M_A}\frac{d}{dt}({}^{\mathbf{A}}V_{\mathrm{r}}) + \mathbf{C_A}({}^{\mathbf{A}}\omega){}^{\mathbf{A}}V_{\mathrm{r}} + \mathbf{G_A}. \tag{4}$$

In Eq. (4), the regressor matrix $\mathbf{Y}_A \in \mathbb{R}^{6\times 13}$ and the parameter vector $\boldsymbol{\theta}_{\mathbf{A}} \in \mathbb{R}^{13}$ are specified in [22].

The required net force/moment vector for the *rigid links* is defined as

$${}^{\mathbf{A}}F_r^* = \mathbf{Y_A}\theta_{\mathbf{A}} + K_{\mathbf{A}}({}^{\mathbf{A}}V_r - {}^{\mathbf{A}}V), \tag{5}$$

where $K_{\mathbf{A}}$ is the velocity feedback control gain.

3 Virtual Decomposition and Kinematics Modeling for the 3-DOF Manipulator

In many industrial applications, it is typical that a mobile working machine with a rigid heavy-duty manipulator is operated in uneven terrain conditions. Varying terrain conditions affect operations, because the orientation of the working machine platform and displacement movements cause a floating-base for the manipulator. Our main focus is to use the VDC approach as a framework to investigate a control design for a hydraulic manipulator with a floating-base. In this paper, it is assumed that the platform movements follow from varying terrain conditions. Further, it is assumed that platform actuators cannot be used to compensate for the floating-base movements of the manipulator base. Considering that the platform movements follow from the environment, it is assumed that there are no constraints on these movements.

As reported in [13], the VDC framework has been used to achieve high control performance for hydraulic manipulators. The VDC the control equations for the complex robot system to be designed locally at the subsystem level [21]. However, in previous studies [8, 10], a 2-DOF manipulator with a fixed-base was examined and a 3-DOF manipulator with a fixed-base was examined in [15].

Next, the three main steps of the VDC framework control design are presented as follows: 1) the coordinate frame attachment to subsystems, 2) virtual decomposition of the entire manipulator system, and 3) presentation of the simple oriented graph (SOG). Finally, the kinematic equations of the 3-DOF manipulator are presented for the control design.

3.1 Virtual Decomposition of the 3-DOF Manipulator

To describe the kinematics and dynamics relations of the subsystems, fixed coordinate frames need to be attached to the rigid bodies. The coordinate frames for 3-DOF manipulator are presented in Fig. 1(a). Then, the entire system needs to be virtually decomposed into subsystems, which are called open chains and objects, by placing conceptual virtual cutting points (VCPs) in the examined system. VCPs comprise directed separation points between successive subsystems for the six-dimensional force/moment related to these subsystems. A VCP is simultaneously interpreted as driving one subsystem and being driven for another. The driven VCP is the point to which the force/moment is exerted, and the driving VCP is the point from which the force/moment vector is exerted. Virtual decomposition for the manipulator is presented in Fig. 1(b).

The dynamics between successive subsystems in a virtual decomposition system can be represented as a SOG (see definition 2.14 in [22]). The SOG describes force/moment directions as directed edges, and the rigid links are described as nodes. The SOG for the manipulator is presented in Fig. 1(c). In view of [22], the platform's relation to a fixed-inertial frame is described with a massless virtual manipulator, which has one VCP with the platform. The virtual manipulator is used to describe the interaction force from the environment to the platform.

The VDC enables modular control design on subsystem level; thus, subsystems can be connected in a plug-and-play manner to other designed subsystems. The VDC control design for the 2-DOF manipulator is presented detail in [6], and the control design for a 3-DOF manipulator with a base rotation is given in [15]. The dynamics model for the hydraulic cylinder is specified in [11, 22], with the corresponding modular control equation. Considering the control design for the manipulator in Fig. 1(b), the floating-base does not affect the control equations for manipulator subsystems.

3.2 Kinematics Modeling for the 3-DOF Manipulator

In robotics applications, the desired manipulator end-effector motions are typically provided as a reference trajectory to the control system. In the VDC approach, the control objective is to make the controlled actual veloc-

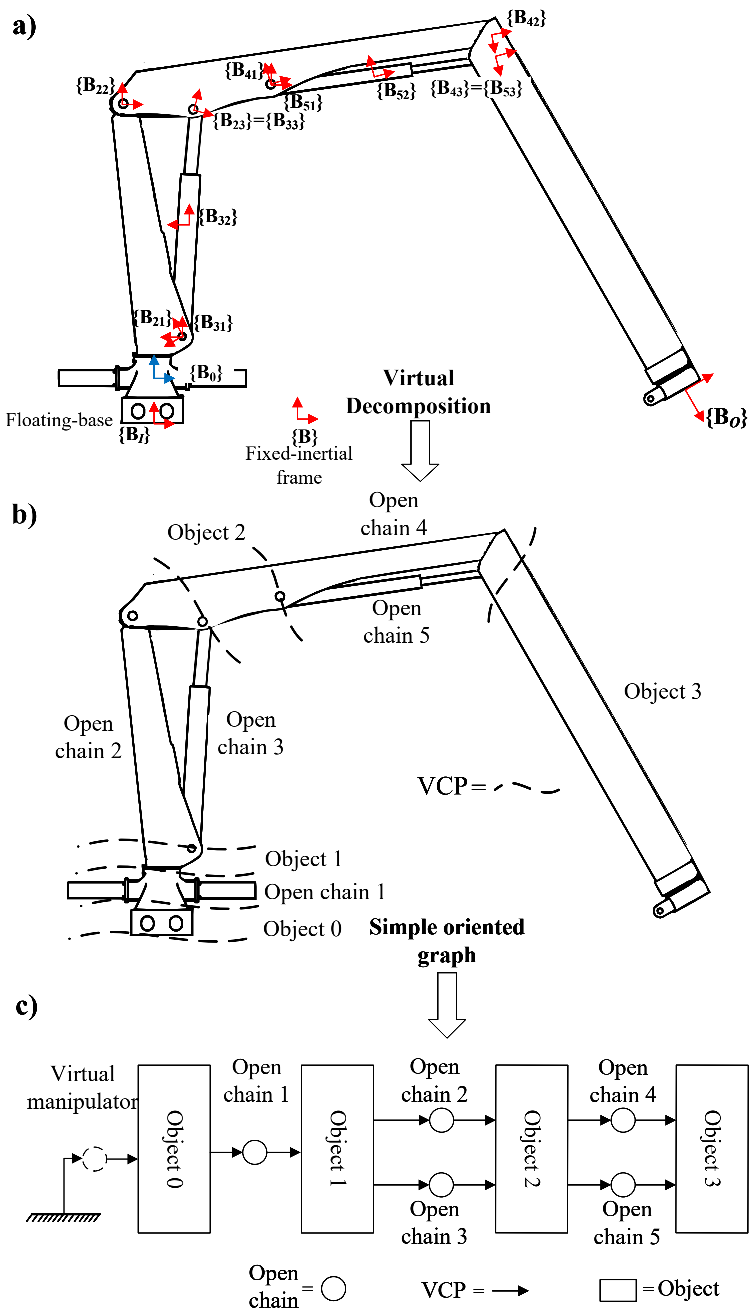

Figure 1 Virtual decomposition for the entire manipulator.

Table 1 DH-parameters for a Three-Bar Manipulator

a	d	α	θ
0	L_0	$-\pi/2$	0
L_{11}	L_{12}	$\pi/2$	θ_1
L_1	0	0	θ_2
L_2	0	0	θ_3

ities track with the required velocities, which consist of the desired velocity and one or more terms that are related to control errors [22]. This can be performed either in the Cartesian space or in joint space. As demonstrated in [7], the VDC approach provides high control performance in the Cartesian space. By considering the manipulator with the floating-base in Fig. 1(a), the platform movements need to incorporate to in the Cartesian space reference design.

The kinematic chain of spatially rigid links in a mechanical system can be modeled using Denavit–Hartenberg (DH) parameters to describe the convention between coordinate frames as a function of the joint angles. The coordinate frames required to describe the kinematics in joint space are given in Fig. 2. These frames are set according to the right-hand rule, so that in blue frames, the y-axis points through the paper, and in other frames, the z-axis points out from the paper. Thus, the kinematics of the manipulator in Fig. 2 can be defined with the DH-parameters in Table 1. The parameters L_{11}, L_{12}, L_0, L_1, and L_2 describe the constant lengths of the rigid links and the joint angles θ_1, θ_2, and θ_3, which are assumed to the measured. In addition, a linear/angular velocity vector in the floating-base coordinate frame $\{\mathbf{B}_I\}$ is assumed to be measured related to the fixed-inertial frame $\{\mathbf{B}\}$.

Comparing the coordinate frames in Fig. 1(a) and Fig. 2, in the latter figure, frames are defined according to DH-parameters. This enables more compact kinematic equations. However, as shown in [9], the rotations for the coordinate frames in Fig. 1(a) can be written according to the joint angles.

The manipulator kinematics can be analyzed by defining the linear/angular velocities in the defined coordinate frames in Fig. 2. Now, by using the DH-parameters in Table 1 and by reusing Eq. (1), the kinematics

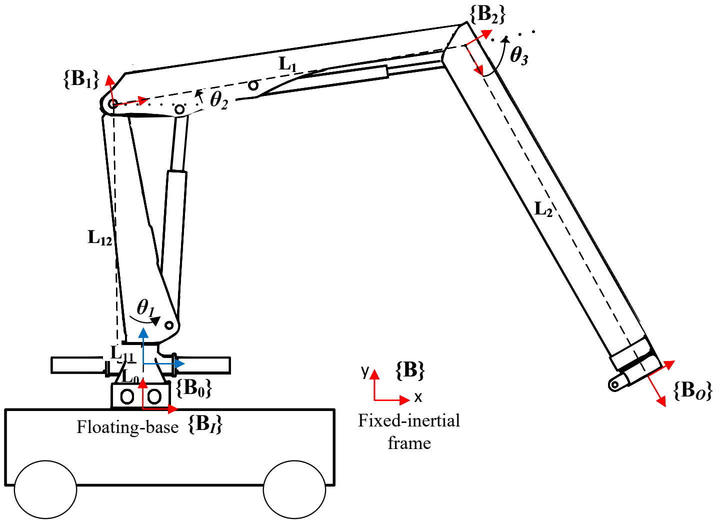

Figure 2 A floating-base mobile manipulator.

for the manipulator can be written as

$$
\begin{aligned}
{}^{\mathbf{B}_0}V &= {}^{\mathbf{B}_I}\mathbf{U}_{\mathbf{B}_0}^{T}\,{}^{\mathbf{B}_I}V + \mathbf{z}\dot{\theta}_1 && (6)\\
{}^{\mathbf{B}_1}V &= {}^{\mathbf{B}_0}\mathbf{U}_{\mathbf{B}_1}^{T}\,{}^{\mathbf{B}_0}V + \mathbf{z}\dot{\theta}_2 && (7)\\
{}^{\mathbf{B}_2}V &= {}^{\mathbf{B}_1}\mathbf{U}_{\mathbf{B}_2}^{T}\,{}^{\mathbf{B}_1}V + \mathbf{z}\dot{\theta}_3 && (8)\\
{}^{\mathbf{B}_O}V &= {}^{\mathbf{B}_2}\mathbf{U}_{\mathbf{B}_O}^{T}\,{}^{\mathbf{B}_2}V, && (9)
\end{aligned}
$$

where $\dot{\theta}_1$, $\dot{\theta}_2$, and $\dot{\theta}_3$ are the angular velocities of the manipulator joints and $\mathbf{z} = [0\ 0\ 0\ 0\ 0\ 1]^T$. In Eq. (6), ${}^{\mathbf{B}_I}V$ is the linear/angular velocity vector for the platform. In this study, it is assumed that the platform velocities can be measured.

3.3 Required Kinematics of the 3-DOF Manipulator

The corresponding equations for the control design can be written by reusing Eqs. (6)–(9), as

$$
\begin{aligned}
{}^{\mathbf{B}_0}V_r &= {}^{\mathbf{B}_I}\mathbf{U}_{\mathbf{B}_0}^{T}\,{}^{\mathbf{B}_I}V_r + \mathbf{z}\dot{\theta}_{1r} && (10)\\
{}^{\mathbf{B}_1}V_r &= {}^{\mathbf{B}_0}\mathbf{U}_{\mathbf{B}_1}^{T}\,{}^{\mathbf{B}_0}V_r + \mathbf{z}\dot{\theta}_{2r} && (11)\\
{}^{\mathbf{B}_2}V_r &= {}^{\mathbf{B}_1}\mathbf{U}_{\mathbf{B}_2}^{T}\,{}^{\mathbf{B}_1}V_r + \mathbf{z}\dot{\theta}_{3r} && (12)\\
{}^{\mathbf{B}_O}V_r &= {}^{\mathbf{B}_2}\mathbf{U}_{\mathbf{B}_O}^{T}\,{}^{\mathbf{B}_2}V_r, && (13)
\end{aligned}
$$

where $\dot{\theta}_{1r}$, $\dot{\theta}_{2r}$, and $\dot{\theta}_{3r}$ are the required joint velocities, and $\mathbf{z} = [0\ 0\ 0\ 0\ 0\ 1]^T$. In the VDC approach, the required actuator dynamics are used to define a feedforward control term for actuators. As Eqs. (4)–(5) show, the required dynamics of the rigid objects in Fig. 2 can be calculated by defining the required velocities, which is a unique property of the VDC. The required angles for the closed-chain subsystem in lift and elbow joints can be written as a function of manipulator joint angles $\dot{\theta}_{1r}$, $\dot{\theta}_{2r}$, and $\dot{\theta}_{3r}$, which are defined in the following section.

4 Cartesian Control for the Floating-Base Manipulator

Considering the mobile working machine with a heavy-duty manipulator, the platform movements during the operation of manipulators affect control design. It is assumed that the automation level of the hydraulic manipulators will rise [13] due to the robotic control of these manipulators. Nowadays, many commercial solutions for these kinds of hydraulic manipulators are available. However, these commercial solutions typically do not consider the effects of platform movements on the end-effector position.

In robotics, it is typical that the desired end-effector motions are investigated in the Cartesian space. However, in hydraulic manipulators, joint space motions are used in the control (see Fig. 2). In view of [23], the forward differential kinematics relation between the Cartesian space and the joint space for the entire examined system can be defined by reusing Eqs. (6)–(9), as

$$\mathbf{J}_q = \left[{}^{\mathbf{B}_0}\mathbf{U}_{\mathbf{B}_O}^T\mathbf{z} \quad {}^{\mathbf{B}_1}\mathbf{U}_{\mathbf{B}_O}^T\mathbf{z} \quad {}^{\mathbf{B}_2}\mathbf{U}_{\mathbf{B}_O}^T\mathbf{z}\right], \tag{14}$$

where $\mathbf{z} = [0\ 0\ 0\ 0\ 0\ 1]^T$, and $\mathbf{J}_q \in \mathbb{R}^{6\times 3}$ is the Jacobian matrix for the manipulator. In Eq. (14), only the forward differential kinematics for the manipulator is presented. Now, by considering the floating-base movements, the forward kinematics of the entire system can be written in a matrix form, as

$$\begin{bmatrix} {}^{\mathbf{B}_O}V \\ {}^{\mathbf{B}_I}V \end{bmatrix} = \begin{bmatrix} \mathbf{J}_q & {}^{\mathbf{B}_I}\mathbf{U}_{\mathbf{B}_O}^T \\ 0 & I_6 \end{bmatrix} \begin{bmatrix} \dot{\mathbf{q}} \\ {}^{\mathbf{B}_I}V \end{bmatrix}, \tag{15}$$

where $\dot{\mathbf{q}} = \left[\dot{\theta}_1\ \dot{\theta}_2\ \dot{\theta}_3\right]^T$ is the joint velocity vector, ${}^{\mathbf{B}_I}V \in \mathbb{R}^6$ is the platform linear/angular velocity vector, and ${}^{\mathbf{B}_O}V \in \mathbb{R}^6$ is the linear/angular velocity vector of the manipulator end-effector.

In Eq. (10)–(13), the forward kinematics describes the relation from the joint space to the Cartesian space. However, in robotics, it is typical that references for the manipulator are defined in Cartesian space. For this reason, the relation between the Cartesin space and the joint space can be defined as inverse kinematics. Considering the 3-DOF manipulator in Fig. 2, only the desired reference values for linear velocities in the coordinate frame $\{\mathbf{B}_O\}$ can be designed in the Cartesian space, and the angular velocities of the end-effector cannot be designed. Therefore, the manipulator end-effector velocity needs to be rewritten, as

$$V_{Or} = \begin{bmatrix} v_{Or} \\ \omega_{Or} \end{bmatrix}, \tag{16}$$

where $v_{Or} \in \mathbb{R}^3$ is the required linear velocity vector, and $\omega_{Or} \in \mathbb{R}^3$ is the required angular velocity in coordinate frame $\{\mathbf{B}_O\}$. Moreover, the Jacobian matrix in Eq. (14) can be rewritten as

$$\mathbf{J}_q = \begin{bmatrix} \mathbf{J}_x \\ \mathbf{J}_\omega \end{bmatrix}, \tag{17}$$

where $\mathbf{J}_x \in \mathbb{R}^{3\times3}$ is the displacement Jacobian and $\mathbf{J}_\omega \in \mathbb{R}^{3\times3}$ is the rotational Jacobian. Now, the inverse solution for manipulator kinematics in the joint space can be written as

$$\dot{\mathbf{q}}_r = \mathbf{J}_x^{-1} v_{Or} - \mathbf{J}_q^{*\mathbf{B}_I} V_r, \tag{18}$$

where ${}^{\mathbf{B}_I}V_r$ is the required platform velocity, and $\dot{\mathbf{q}}_r$ is the required joint velocity vector. In this paper, it is assumed that platform velocities follow directly from environmental changes and are not controllable. Therefore, it can be assumed that ${}^{\mathbf{B}_I}V_r = {}^{\mathbf{B}_I}V$. In Eq. (18), $\mathbf{J}_q^* \in \mathbb{R}^{3\times6}$ is the weighted pseudoinverse solution for the Jacobian inverse. In this study, the inverse solution is calculated by using Moore-Penrose pseudoinverse solution.

In the Cartesian space, the required linear velocity v_{Or} in Eq. (18) can be defined by using the desired linear velocity and the desired end-effector position, as

$$v_{Or} = v_{Od} + \lambda(X_d - X), \tag{19}$$

where $\lambda \in \mathbb{R}^{3\times3}$ is the position feedback gain matrix with diagonal [λ_x λ_y λ_z] for the Cartesian position, $X_d \in \mathbb{R}^3$ and $X \in \mathbb{R}^3$ are the desired and measured Cartesian position values for the manipulator end-effector, and v_{Od} is the desired linear velocity in frame $\{\mathbf{B}_O\}$. Typically, the desired positions and linear velocities are provided as a reference trajectory. In this paper, the measured value for Cartesian position is calculated by using measured joint angles and manipulator kinematics equations.

Table 2 Manipulator main links parameters for simulation

Link	Length	Mass
L_0	0.25 m	20 kg
L_1	1.30 m	50 kg
L_2	2.00 m	50 kg
L_{11}	-0.12 m	0 kg
L_{12}	1.30 m	90 kg

5 Simulation Results

In this section, we discuss how the control equations in Sections 3 and 4 are verified by simulation results. The proposed control equations are simulated in three different test cases. In the first case, it is demonstrated that the proposed control equations can be used to compensate for the effects of the platform angular velocities on the end-effector position. The second simulation results show that the proposed control equations enable the desired velocity of the manipulator end-effector to be designed despite platform movements. In the final case, the effectiveness of the proposed control equations is demonstrated when the platform has linear and angular velocities.

The mechanical model for the floating-base mobile manipulator in Fig. 2 is constructed in the MATLAB Simscape Multibody software environment. This simulation environment provides a multi-body simulation for 3D-mechanical systems, including rigid body inertial parameters, joints, and constraints. In Table 2, the main dimensions and the mass parameters for the manipulator's rigid links are presented. The dimensions for the manipulator's cylinders (see Fig. 2) are $80/60-380$ for the rotation cylinder, $80/60-600$ for the lift cylinder and $80/60-600$ for the elbow cylinder. In simulations, all system measurements are defined to correspond the real-time experimental setup in [15]. The feedback gains in the Cartesian space (see Eq. (19)) are set for each direction as $\lambda_x = \lambda_y = 8$ and $\lambda_z = 14$ are used in all simulation cases.

In the first case, it is assumed that the platform orientation in coordinate frame $\{\mathbf{B}_I\}$ (see Fig. 2) can be changed related to fixed frame $\{\mathbf{B}\}$. The desired linear velocity for the end-effector in frame $\{\mathbf{B}_O\}$ is defined as zero and the reference position is set as fixed to point $[2.92\ 0.97\ 0.1858]^T$. The angular velocities in the floating-base coordinate frame $\{\mathbf{B}_I\}$ are shown in Fig. 3. The corresponding Cartesian space position for the manipulator end-effector is presented in Fig. 4. As the Fig 4 shows, the proposed control equations

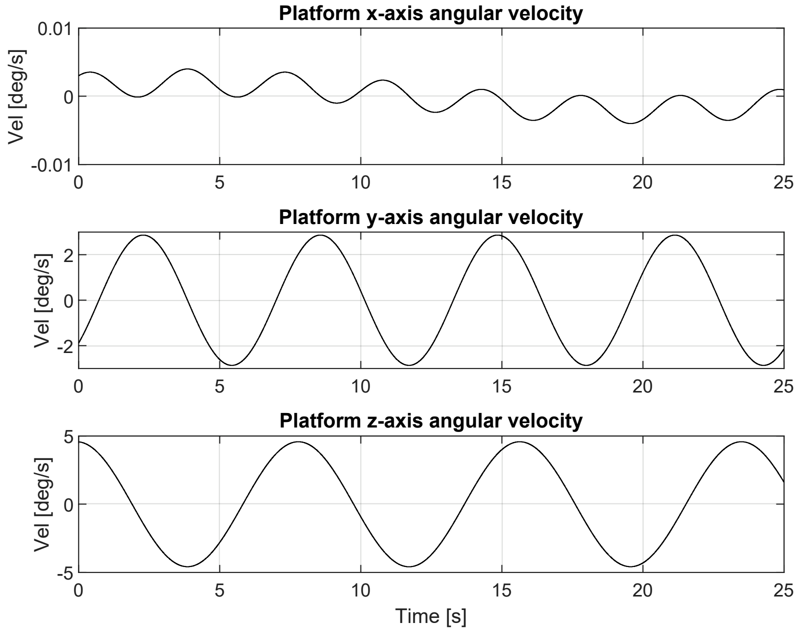

Figure 3 Manipulator floating-base angular velocities.

enable efficiently compensate the floating-base movements by end-effector Cartesian space control.

In the second case, a point-to-point quintic reference trajectory is used to the define desired linear velocity for the end-effector. The end-effector x-axis desired linear velocity in frame $\{\mathbf{B}_O\}$ is designed so that the end-effector moves from point 3.0 m to 2.8 m in a 2 s period, while the other directions are set to constant. The floating-base angular velocities in this case are similarly to the first test case. The corresponding end-effector position is presented in Fig. 5. The results show that the proposed control equations allow us to design an end-effector Cartesian position reference separate from the platform movements. Comparing the simulation the results in Fig. 5 to results in Fig. 4, the manipulator movements does not effect significantly to position tracking errors.

In the final case, it is assumed that the platform also has the linear velocity along the x-axle in coordinate frame $\{\mathbf{B}_O\}$. The platform velocities in this case are presented in Fig. 6, where the angular velocities are the same as in Fig. 3. Similar to the first case, the desired linear velocity for the end-effector

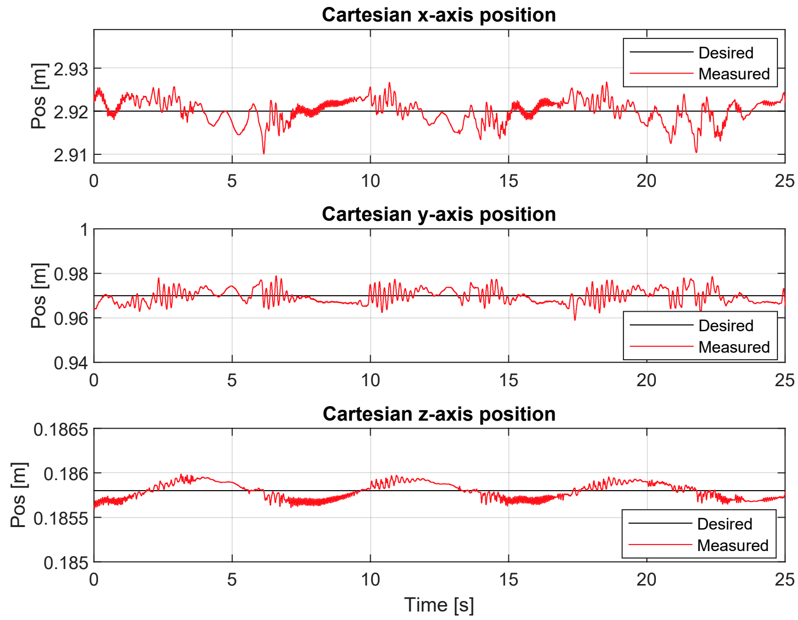

Figure 4 Manipulator end-effector position with a constant reference.

is zero, and the end-effector position is set to $[2.92\ 0.97\ 0.1858]^T$. Now, the end-effector positions with the platform velocities in Fig. 6 are presented in Fig. 7. Comparing the simulation results in Fig. 4 to the results in Fig. 7, also in this case, the proposed control equations enable compensation for platform movements. Considering the tracking errors in Fig. 4 and Fig. 7, the platform linear velocity does not affect the tracking error of the end-effector position.

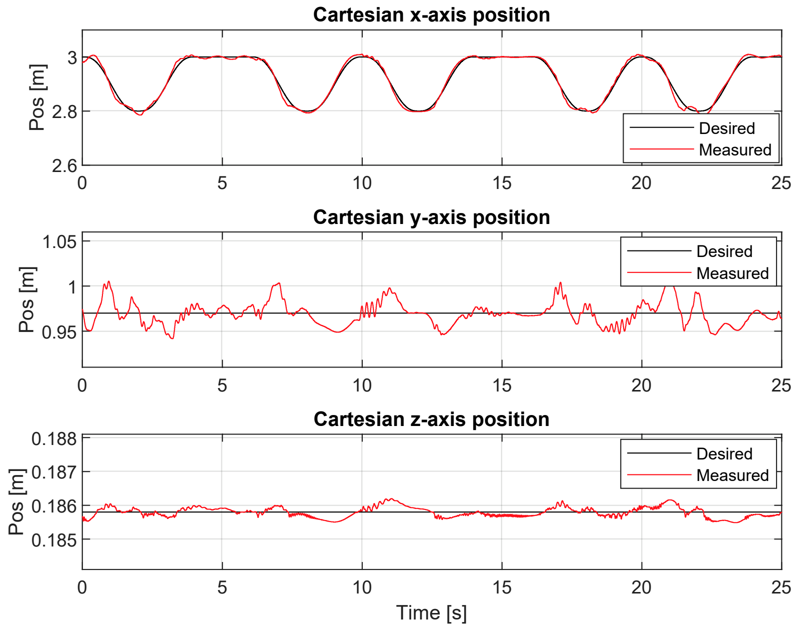

Figure 5 Manipulator end-effector position with motion.

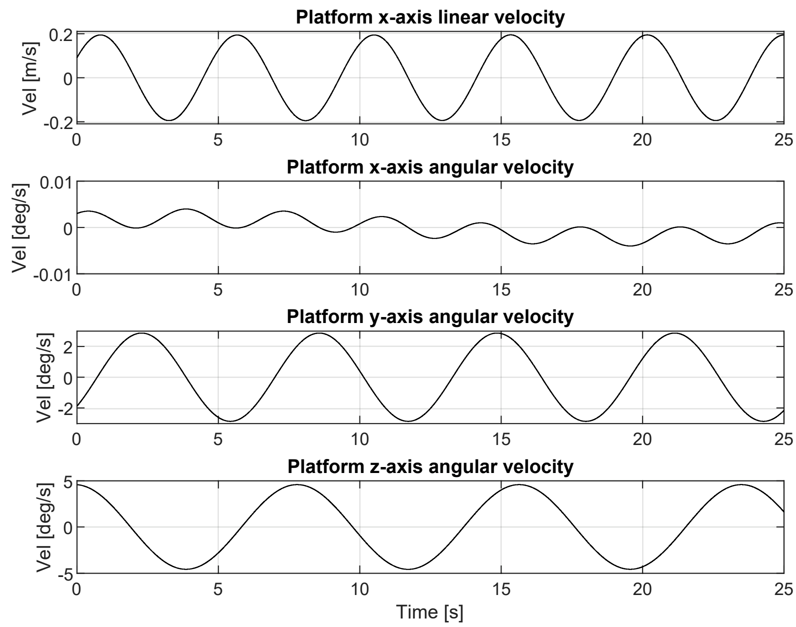

Figure 6 Floating-base linear and angular velocities.

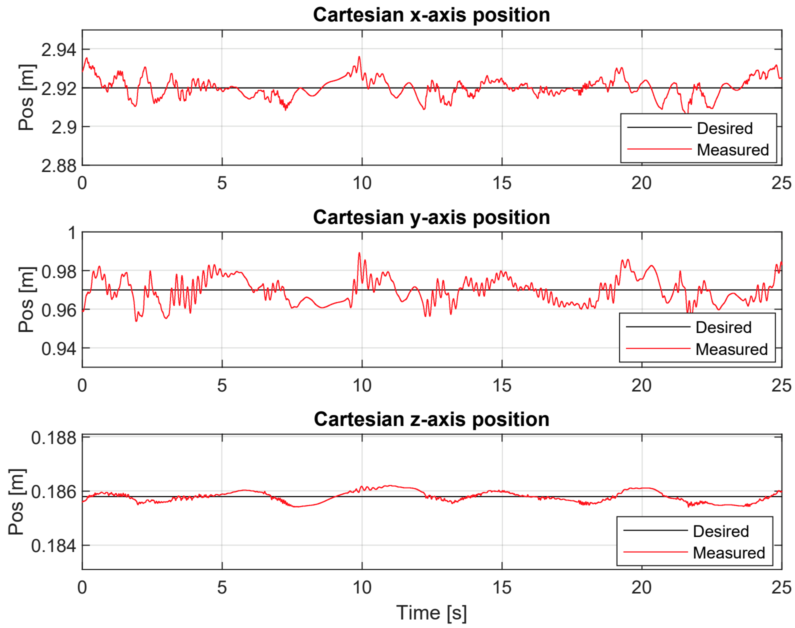

Figure 7 Manipulator end-effector position with a constant reference.

6 Conclusion

This paper's main focus was proposing an NMB controller for a heavy-duty manipulator mounted with a floating-base-like mobile platform. The proposed control equations enables mobile manipulator movements to be handled during end-effector movements. As the simulation results demonstrated, the proposed control equations can be used to compensate for the effects of the platform movements from the manipulator end-effector control design.

The results of this study provided a baseline controller for our future studies, where the proposed controller will be implemented to full-size commercial manipulators, and the experimental results will be presented to verify the effectiveness of the proposed controller.

References

[1] EU. *EU Robotics*. 2018. [online], accessed 23.6.2022, available: Strategic research agenda for robotics in europe 2014–2020.

[2] Raouf Fareh, Mohamad R. Saad, Maarouf Saad, Abdelkrim Brahmi, and Maamar Bettayeb. Trajectory tracking and stability analysis for mobile manipulators based on decentralized control. *Robotica*, 37(10):1732–1749, 2019.

[3] HIAB. *Crane Tip Control*. 2021. [online], accessed 24.6.2022, available: https://www.hiab.com/en/media/news/hiab-crane-tip-control.

[4] Rongyu Jin, Paolo Rocco, and Yunhai Geng. Cartesian trajectory planning of space robots using a multi-objective optimization. *Aerospace Science and Technology*, 108:106360, 2021.

[5] Jouko Kalmari, Juha Backman, and Arto Visala. Nonlinear model predictive control of hydraulic forestry crane with automatic sway damping. *Computers and Electronics in Agriculture*, 109:36–45, 2014.

[6] Janne Koivumäki and Jouni Mattila. High performance nonlinear motion/force controller design for redundant hydraulic construction crane automation. *Automation in Construction*, 51:59–77, 2015.

[7] Janne Koivumäki and Jouni Mattila. Stability-guaranteed force-sensorless contact force/motion control of heavy-duty hydraulic manipulators. *IEEE Trans. Robotics*, 31(4):918–935, 2015.

[8] Janne Koivumäki and Jouni Mattila. Stability-guaranteed impedance control of hydraulic robotic manipulators. *IEEE/ASME Trans. Mechatronics*, 22(2):601–612, 2017.

[9] Janne Koivumäki, Wen-Hong Zhu, and Jouni Mattila. Addressing closed-chain dynamics for high-precision control of hydraulic cylinder actuated manipulators. In *BATH/ASME 2018 Symposium on Fluid Power and Motion Control*, pages V001T01A018–V001T01A018. ASME, 2018.

[10] Janne Koivumäki, Wen-Hong Zhu, and Jouni Mattila. Energy-efficient and high-precision control of hydraulic robots. *Control Engineering Practice*, 85:176–193, 2019.

[11] Santeri Lampinen, Janne Koivumäki, and Jouni Mattila. Improved hydraulic cylinder model for the virtual decomposition control approach. In *2019 IEEE International Conference on Cybernetics and Intelligent Systems (CIS) and IEEE Conference on Robotics, Automation and Mechatronics (RAM)*, pages 113–118. IEEE, 2019.

[12] Santeri Lampinen, Janne Koivumäki, Wen-Hong Zhu, and Jouni Mattila. Force-sensorless bilateral teleoperation control of dissimilar master-slave system with arbitrary scaling. *IEEE Transactions on Control Systems Technology*, pages 1–15, 2021.

[13] Jouni Mattila, Janne Koivumäki, Darwin G Caldwell, and Claudio Semini. A survey on control of hydraulic robotic manipulators with projection to future trends. *IEEE/ASME Trans. on Mechatronics*, 22(2):669–680, 2017.

[14] Pauli Mustalahti, Janne Koivumäki, and Jouni Mattila. Stability-guaranteed anti-sway controller design for a redundant articulated hydraulic manipulator in the vertical plane. In *ASME/BATH Symp. on Fluid Power and Motion Control*, pages V001T01A031–V001T01A031. ASME, 2017.

[15] Pauli Mustalahti and Jouni Mattila. Nonlinear model-based controller design for a hydraulic rack and pinion gear actuator. In *BATH/ASME 2018 Symp. on Fluid Power and Motion Control*, pages V001T01A020–V001T01A020. ASME, 2018.
[16] Pauli Mustalahti and Jouni Mattila. Nonlinear model-based control design for a hydraulically actuated spherical wrist. In *Fluid Power Systems Technology*, volume 59339, page V001T01A027. American Society of Mechanical Engineers, 2019.
[17] Jörg Neupert, Eckhard Arnold, Klaus Schneider, and Oliver Sawodny. Tracking and anti-sway control for boom cranes. *Control Engineering Practice*, 18(1):31–44, 2010.
[18] Ponsse. *Active Crane*. 2021. [online], accessed 24.6.2022, available: https://www.ponsse.com/en/web/guest/products/tailored-solutions/product/-/p/activecranebisonbuffaloelephant.
[19] Geir Ole Tysse, Andrej Cibicik, Lars Tingelstad, and Olav Egeland. Lyapunov-based damping controller with nonlinear mpc control of payload position for a knuckle boom crane. *Automatica*, 140:110219, 2022.
[20] J. Watton. *Fluid Power Systems: modelling, simulation, analog and microcomputer control*. Prentice Hall, New York, 1989.
[21] W.-H. Zhu, Y.-G. Xi, Z.-J. Zhang, Z. Bien, and J. De Schutter. Virtual decomposition based control for generalized high dimensional robotic systems with complicated structure. *IEEE Trans. Robot. Autom.*, 13(3):411–436, 1997.
[22] Wen-Hong Zhu. *Virtual decomposition control: toward hyper degrees of freedom robots*, volume 60. Springer Science & Business Media, 2010.
[23] Wen-Hong Zhu and Joris De Schutter. Adaptive control of electrically driven space robots based on virtual decomposition. *Journal of guidance, control, and dynamics*, 22(2):329–339, 1999.

Biography

Pauli Mustalahti received the M.Sc. degree in engineering from the Tampere University of Technology in 2016 and the D.Sc. (Tech.) in Automation Science and Engineering from the Tampere University in 2023. He is a researcher in the Automation Technology and Mechanical Engineering, Tampere University, Tampere, Finland. His research interests include nonlinear model-based control of robotic manipulators.

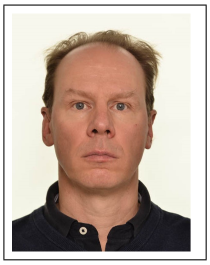

Jouni Mattila received his M.Sc. in 1995 and Dr. Tech in 2000, both from Tampere University of Technology (TUT), Tampere, Finland. He is currently a professor of machine automation with the unit of Automation Technology and Mechanical Engineering, Tampere University. His research interests include machine automation, nonlinear model-based control of robotic manipulators and energy-efficient control of heavy-duty mobile manipulators.